Crystal structures and conformational effects in bis-fluorenyl based ligands and related ruthenium nitrosyl complexes

Yael Juarez-Martinez, Pablo Labra-Vázquez, Pascal G. Lacroix, Marine Tassé, Mathilde Bocé, Sonia Mallet-Ladeira, Isabelle Malfant

Crystal structures and conformational effects in bis-fluorenyl based ligands and related ruthenium nitrosyl complexes

Yael Juarez-Martinez, Pablo Labra-Vázquez, Pascal G. Lacroix*, Marine Tassé, Mathilde Bocé, Sonia Mallet-Ladeira, Isabelle Malfant*

Laboratoire de Chimie de Coordination du CNRS, 205 route de Narbonne, F-31077 Toulouse, France.

Abstract

Four crystal structures (two ruthenium complexes and two ligands) are presented containing a *bis*-fluorene fragment on which alkyl chains (methyl and hexyl) are grafted. The possibility to get both *cisoid* and *transoid* conformations in the *bis*-fluorene units is discussed. A computational investigation using the density functional theory indicates a tendency for a gradual stabilization of the *cisoid* form, as the length of the chains increases. The effect of the conformation on the charge transfer electronic properties of *bis*-fluorene based materials is discussed computationally at one-photon absorption (OPA) level and tentatively at two-photon absorption (TPA) levels, but it is found to be modest.

Keywords: Two-photon absorption, ruthenium nitrosyl, ligand design, nitric oxide, DFT computation.

1. Introduction

Nitric oxide (NO•) is a short-lived radical, which plays multiple roles in mammalian physiology (e.g. regulator of cardiovascular function, metabolism, neurotransmission, immunity among others) [1-5]. Due to these numerous functions, exogeneous NO• donors have been intensively investigated for various potential therapeutic applications [6-11].

Something important to note about nitric oxide is its inherent toxicity and furthermore the fact this its action in tissues depends on its concentration [12-15]. For these reasons, ruthenium nitrosyl (RuNO) complexes appear especially appealing due to their capability to release NO• locally and quantitatively under light irradiation in the λ = 300-500 nm domain, taking advantage of the non-invasive and highly controllable characteristics of light [16-20]. However, and to be fully applicable, the NO• release should be achieved in the λ = 600 – 1300 nm therapeutic window of relative transparency of biological tissues [21]. To overpass this difficulty, the NO release occurring by one-photon absorption (OPA) in the λ = 300-500 nm domain may be achieved by the use of two-photon absorption (TPA) technique, which uses two photons of half-energy instead of one, in the λ = 600-1000 nm domain, and therefore has gained a widespread popularity in the biology community as an extremely powerful tool for local photoactivation and drug delivery [22,23].

Following this strategy, our team has been engaged in a research program dedicated to the investigation of RuNO complexes built up from fluorenyl-terpyridine ligands (**FC_6TRubpyNO**, Scheme 1) [24]. The choice of the fluorene is due to the charge transfer character induced from this electron-rich unit to the strongly withdrawing NO ligand. Indeed, it is well recognized that intense charge transfer transitions are the basis of TPA molecules with enhanced capabilities [25-27]. However, it has long been observed that the concept of symmetric charge transfer leads to large enhancement of the TPA response [28]. Along this line, species such as ***bis*-(FC_6TRubpyNO)** (Scheme 2) offer appealing perspectives [29].

* *Corresponding authors E-mail: pascal.lacroix@lcc-toulouse.fr, isabelle.malfant@lcc-toulouse.fr*

For solubility reason required to perform the TPA investigations, the RuNO complexes with two fluorene units investigated in our group contain 4 hexyl chains, which hampers most of the attempts for obtaining crystal structures. To overpass this difficulty, we present here a strategy aiming at using methyl instead of hexyl in the design of the fluorene ligands. This strategy allowed us to get three crystal structures for the dimethylfluorenyl-based molecules labelled **TFFT**, **FFT** and **FFTRuCl$_2$NO** (Scheme 1). They will be presented with that of an intermediate obtained during the synthesis of the targeted complex **FFC$_6$TRubpyNO** (Scheme 1), in which NO is replaced by a nitrito (NO_2^-) ligand. The issue of the (*cisoid* / *transoid*) conformation in the *bis*-fluorene moieties, which arises naturally from the examination of the structures, will be discussed computationally in relation to the optical properties at the OPA and TPA levels.

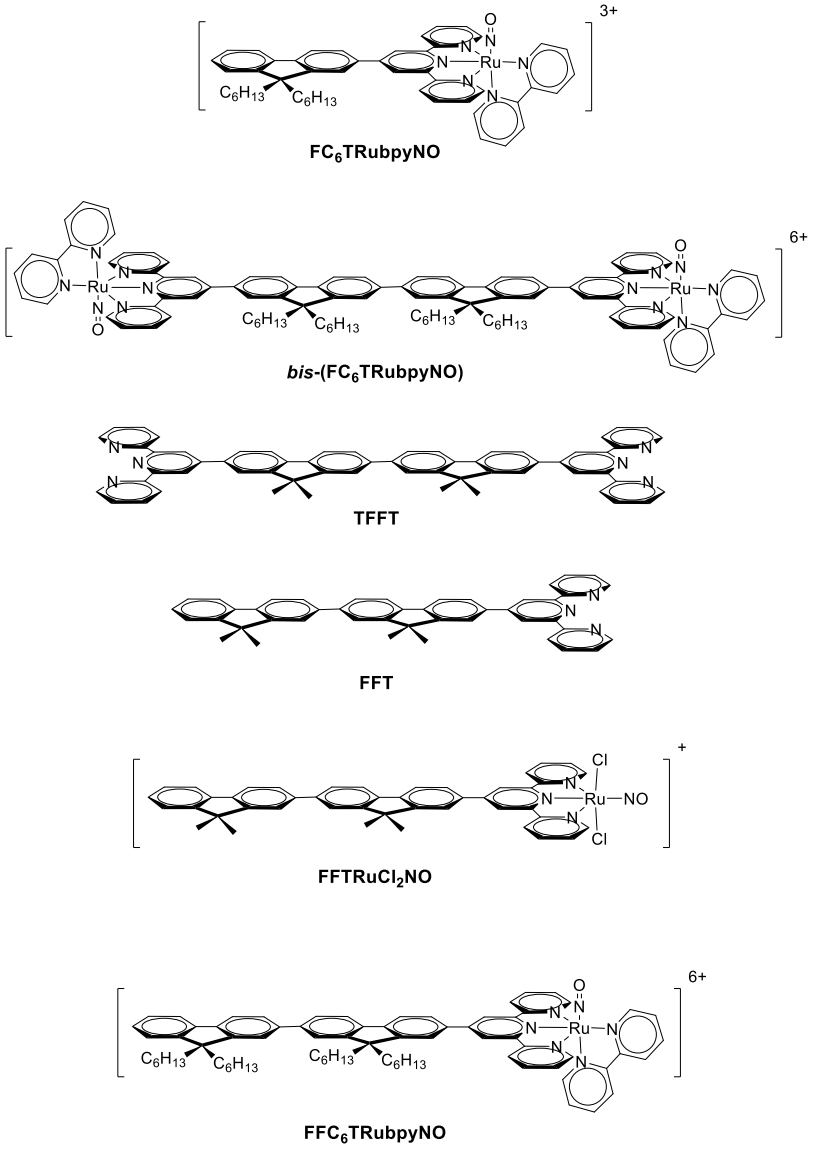

Scheme 1. Ligands and ruthenium-nitrosyl complexes containing the fluorenylterpyridine fragment. In the present scheme, the *bis*-fluorenyl fragments are drawn in the *cisoid* conformation.

2. Results and discussion

2.1. Synthesis and characterization

The desired ligands **TFFT** and **FFT** were synthesized through multi-step reaction sequences, as depicted in Schemes 2 and 3. To address the acidity of the protons at position C-9 in non-substituted fluorene (Scheme 2), which could potentially interfere with subsequent steps involving basic media, methyl chains were introduced at that specific position [30]. This choice for methylated chain was strategically made to promote crystal formation, as methyl chains have shown a higher propensity for generating crystals compared to hexyl chains, which are typically employed for improved solubility. Incorporating methyl chains aids in minimizing disorder within the crystal lattice, thereby facilitating the formation of more organized and precisely defined structures.

The synthesis of ligand **TFFT** started with the aldol condensation between aldehyde **1** and 2-acetylpyridine, yielding enone **2**. Compound **2** underwent by Kröhnke terpyridine synthesis method [31] starting through addition with the enolate of pyridinium salt, resulting in the formation of compound **3**,. The brominated terpyridine **3** was then utilized in Suzuki-Miyaura cross-coupling reactions as the key final synthetic steps, employing pinacolboryl terpyridine **4** as the coupling partner. In this final step, the addition of dichloromethane was necessary due to the compound's low solubility in the toluene/ethanol mixture.

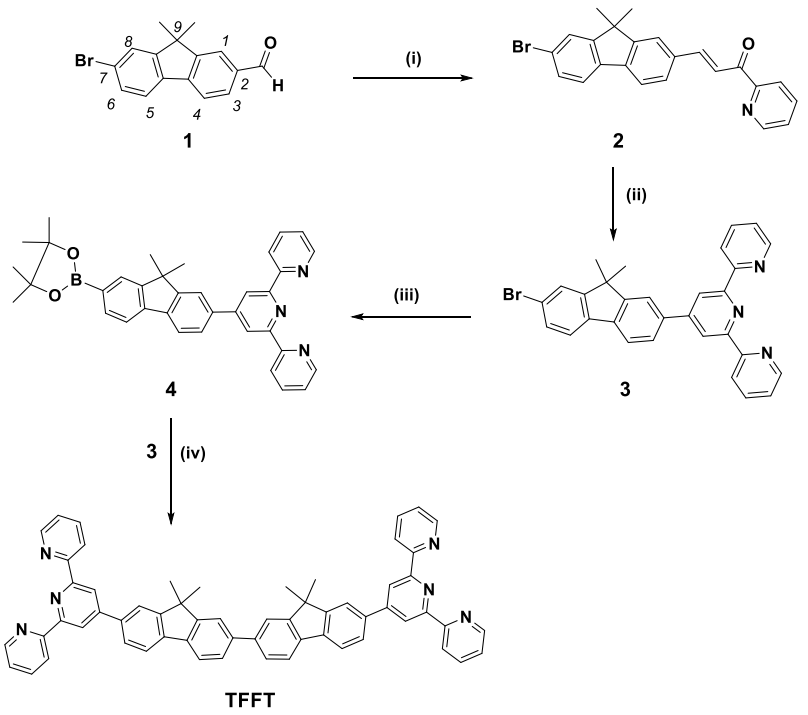

Scheme 2. Synthesis of **TFFT** Reagents and conditions: (i) 2-acetylpyridine, NaOH, EtOH/H_2O/THF, r.t. (66 %); (ii) 1-[2-oxo-2-(2-pyridinyl)ethyl]pyridinium iodide NH_4OAc, EtOH/THF, reflux (54 %), (iii) $Pd(dppf)Cl_2$·DCM, B_2pin_2, KOAc, DMSO, 130°C (62 %); (iv) $Pd(dppf)_2Cl_2$, K_2CO_3, TBAB, toluene/EtOH/DCM, reflux (25 %).

Ligand **FFT** was synthesized in a similar manner, starting from compound **5** which was transformed into the final compound through a Miyaura cross-coupling reaction with compound **4**. The identities of the synthesized compounds were successfully confirmed using $^{1}H/^{13}C$NMR and HRMS techniques.

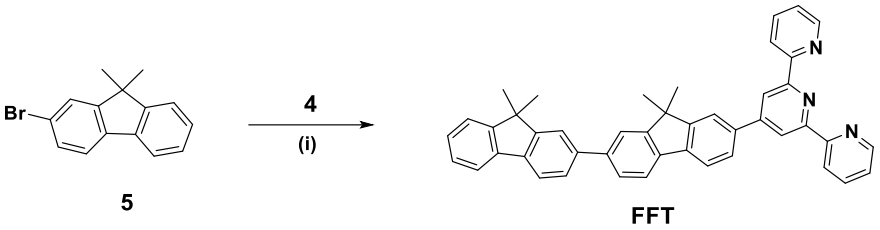

Scheme 3. Synthesis of ligand **FFT**. Reagents and conditions: (i) $Pd(dppf)_2Cl_2$, K_2CO_3, TBAB, toluene/EtOH, reflux (45 %).

The synthesis **of FFTRuCl$_2$NO** was achieved using our previously reported methodology in which the ruthenium atom is introduced by reaction of the ligand with $RuCl_3$ followed by bubbling of NO gas, freshly produced by reaction of HNO_3 on copper wires [32]. The two *cis*(Cl,Cl) and *trans*(Cl,Cl) isomers are separated by HPLC.

The Infra-red *v*NO frequencies for the *cis*(Cl,Cl) and *trans*(Cl,Cl) isomers are equal to 1897 cm^{-1} and 1904 cm^{-1}, respectively. These values are comparable to those recorded in the related complex **FTRuCl$_2$NO** containing a single fluorene: 1894 cm^{-1} for the *cis*(Cl,Cl) and 1901 cm^{-1} for the *trans*(Cl,Cl) complexes [32(a)]. However, the difference is more pronounced with those recorded in **FC$_6$TRubpyNO** (1942 cm^{-1}) ***bis*-(FC$_6$TRubpyNO)** (1937 cm^{-1}) and **FFC$_6$TRubpyNO** (1938 cm^{-1} [29]). The *v*NO frequencies is largely influenced by the amount of electron density transferred to the withdrawing NO group through a RuNO d-π* overlap. While bipydine ligands are capable of significant d-π* back donation, with a concomitent lowering of the electron density on the Ru^{II} atom, the presence of the chlorido ligands increases the electron density, the charge transfer to the π* orbital of the NO fragment, which leads to a decrease of the bond order and finally decrease of the *v*NO frequency.

2.2. UV-visible spectroscopy

Figure 1 gathers the UV-visible spectra of the *cis*/*trans*(Cl,Cl)-**FFTRuCl$_2$NO** complex with that of the related **FFT** ligand. For solubility reason, the spectrum of the ligand was recorded in chloroform and those of the complexes in acetonitrile.

FFT exhibits two absorption maxima at λ = 345 nm (ε = 53 700 mol^{-1} L cm^{-1}) and λ = 293 nm (ε = 26 400 mol^{-1} L cm^{-1}). The RuNO complexes exhibit two bands with absorption maxima located at 434 nm (ε = 9 300 mol^{-1} L cm^{-1}) and at 328 nm (ε = 20 100 mol^{-1} L cm^{-1}) with a shoulder at ~290 nm for the *cis*(Cl,Cl)-**FFTRuCl$_2$NO**, and at 450 nm (ε = 9 150 mol^{-1} L cm^{-1}) and at 330 nm (ε = 19 400 mol^{-1} L cm^{-1}) with a shoulder at ~300 nm for the *trans*(Cl,Cl)-**FFTRuCl$_2$NO**. The comparison between ligand and complexes spectra is strongly reminiscent of that carried out on the related **FTRuCl$_2$NO** containing a single fluorene [32(a)]: (*i*) general trend for reduced intensity transition in the complexes compared to those of the related ligand ; (*ii*) appearance of new transitions at lower energy ascribable to a charge transfer between the electron rich fluorene and the withdrawing RuNO fragment.

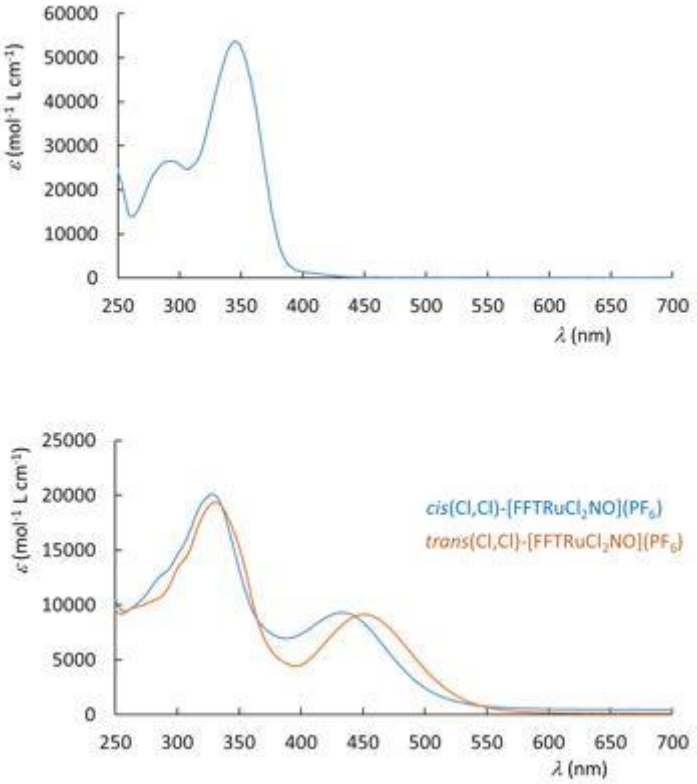

Fig. 1 Experimental UV-visible spectra for **FFT** in chloroform (top) and the related **FFTRuCl$_2$NO** complexes in acetonitrile (bottom).

The UV-visible spectrum of **TFFT** is presented in Supplementary Material. It appears grossly similar to that of **FFT**, with absorption maxima at λ = 356 nm (ε = 65 400 mol^{-1} L cm^{-1}) and λ = 287 nm (ε = 36 800 mol^{-1} L cm^{-1}). Both redshift and enhanced intensities appear consitent with the increase of the size of the π-delocalized electronic structure in **TFFT**.

2.3. Crystal structures

The four compounds **FFT**, **TFFT**, **FFTRuCl$_2$NO**, and **FFC$_6$TRubpyNO$_2$** crystallize in the triclinic P-1 space group, in which two molecular units refer to one-another by an inversion center. Their asymmetric unit cells are shown in Figure 2, 3, 4, and 5, respectively. The main crystal data for the four reported crystal structures are presented in Table 1.

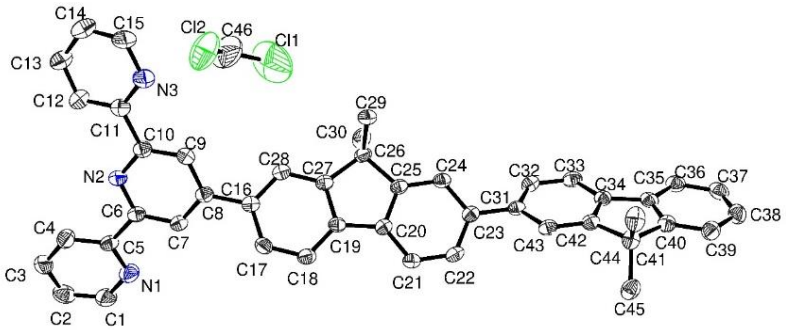

Fig. 2 Asymmetric unit cell for **FFT** with atom labelling scheme. Displacement ellipsoids are drawn at the 50% probability level. Hydrogen atoms are omitted for clarity.

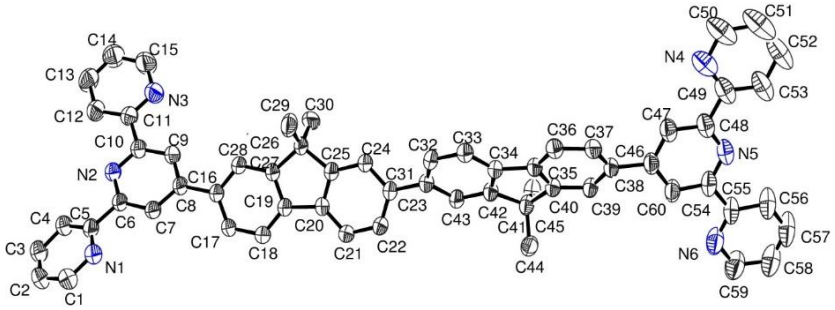

Fig. 3 Asymmetric unit cell for **TFFT** with atom labelling scheme. Displacement ellipsoids are drawn at the 50% probability level. Hydrogen atoms are omitted for clarity.

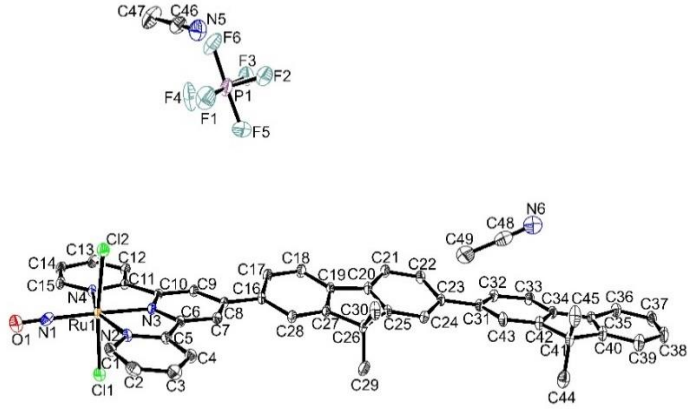

Fig. 4 Asymmetric unit cell for **FFTRuCl$_2$NO** with atom labelling scheme. Displacement ellipsoids are drawn at the 50% probability level. Hydrogen atoms are omitted for clarity.

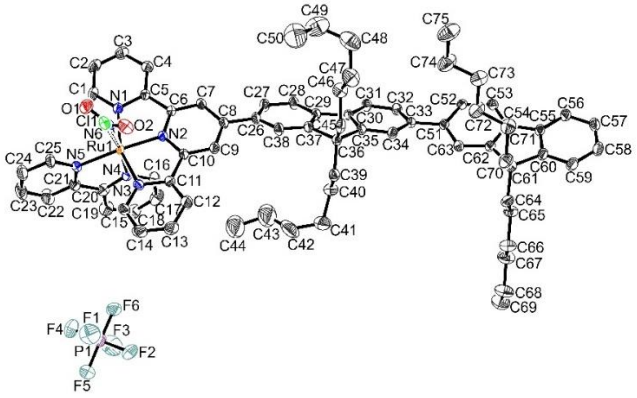

Fig. 5 Asymmetric unit cell for **FFC$_6$TRubpyNO$_2$** with atom labelling scheme. Displacement ellipsoids are drawn at the 50% probability level. Hydrogen atoms are omitted for clarity.

Table 1 Cystallographic data for *bis*-fluorene containing species.

	FFT	**TFFT**	**FFC$_6$TRubpyNO2**	**FFTRuCl2NO**
Color	colorless	pink	orange	red
Chemical Formula	$C_{45}H_{35}N_3$, 0.5 CH_2Cl_2	$C_{60}H_{44}N_6$	$C_{75}H_{83}$ $Cl_{0.16}N_{5.84}O_{1.68}Ru$, F_6P	$C_{45}H_{35}Cl_2N_4ORu$, F_6P, 2 C_2H_3N
Formula weight	660.22	849.01	1344.85	1046.82
Crystal system	triclinic	triclinic	triclinic	triclinic
Space group	P-1	P-1	P-1	P-1
T (K)	133(2)	180(2)	193(2)	100(2)
Wavelength (Å)	0.71073 (MoKα)	1.54184 (CuKα)	0.71073 (MoKα)	0.71073 (MoKα)
a (Å)	9.9896(15)	9.6440(6)	10.6127(8)	11.6939(12)
b (Å)	12.578(2)	14.7061(9)	13.2976(10)	13.6871(13)
c (Å)	14.548(2)	19.0602(11)	24.8420(19)	16.3467(16)
alpha (°)	107.935(5)	107.209(5)	95.125(2)	74.716(3)
beta (°)	97.369(5)	100.924(5)	98.326(2)	73.022(4)
gamma (°)	92.078(5)	100.765(5)	91.055(3)	64.856(4)
Z	2	2	2	2
$D_{calc.}$ (g cm^{-3})	1.275	1.151	1.293	1.555
Abs. coef. (mm^{-1})	0.149	0.528	0.321	0.577
Data collected	51627	25924	90987	80026
Unique	5874 [R_{int} = 0.1325]	9339 [R_{int} = 0.0519]	17263 [R_{int} = 0.0768]	11984 [R_{int} = 0.0632]
Parameters	465	599	979	601
R_1[a] [I>2sigma(I)]	0.0604	0.0618	0.0461	0.0442
wR_2[b] (all data)	0.1534	0.1891	0.1042	0.1164

refinement	F^2	F^2	F^2	F^2
GOF (F^2)	1.017	0.970	1.026	1.076

[a] $R_1 = \sum\big||F_0| - |F_C|\big|/\sum|F_0|$

[b] $wR_2 = \ [\sum[w(F_0^2 - F_C^2)^2]/\sum[(wF_0^2)^2]]^{1/2}$

In the case of **FFT** (Figure 2), an additional molecule of dichloromethane is present in the asymmetric unit cell. The terpyridine fragment (18 heavy atoms) is nearly planar, however with largest deviation of 0.370 Å to the mean plane observed at C4. The torsion angles between the terpyridine (18 heavy atoms) and the planar adjacent fluorene (13 heavy atoms) is equal to 39.78° and the torsion angle between the two fluorenes is equal to 44.05 Å. These large torsion angles suggest the absence of significant packing effects. It is observed 23 short contacts with neighboring molecules (less than the sum of Van der Waals radii). The shortest intermolecular contact is equal to 2.373 Å (H13⋯H39).

The asymmetric unit cell of **TFFT** shown in Figure 3 reveals that the molecular structure is far from being symmetrical. In particular, if one teryridine can be regarded as planar (C46 – C59), the second one (C1 – C15) is significantly distorted with largest deviation to mean plane equal to 0.427 Å, at N1. The torsion angle between terpyridine fragments (18 atoms) and fluorene fragments (13 atoms) are as follows: 27.05° between terpyridine C1 – C15 and fluorene C16 – C26; 33.46° between terpyridine C46 – C59 and fluorene C31 – C41. The torsion angle between the two fluorenes is equal to 49.09°, which indicates a modest overlap between the π-electron cores of each fluorene. It is observed 39 short contacts between one **TFFT** entity and neighboring molecules.

The asymmetric unit cell of **FFTRuCl$_2$NO** is shown in Figure 4. The presence of a PF_6^- anion indicates a charge +1 for the complex, which leads to ruthenium atoms present as Ru^{II}. Two molecules of acetonitrile are evidenced in the unit cell. The coordination sphere of the Ru^{II} atom corresponds to the *trans*(Cl,Cl) isomer. Contrary to the situation encountered in the free **FFT** ligand, the two fluorene units are in *cisoid* conformations in the complex. The three conjugated fragments are nearly planar, with torsion angle between terpyridine et fluorene mean planes equal to 14.59°, and 15.15° between the two fluorene units, which may favor a long-range electron delocalization towards the withdrawing NO group. Up to 46 short contacts are observed between each **FFTRuCl$_2$NO** entity and neighboring molecules.

Finally, the unit cell of **FFC$_6$TRubpyNO$_2$** is shown in Figure 5. The fact to investigate crystals of ruthenium nitrite ($RuNO_2$) complexes instead of ruthenium nitrosyl (RuNO) complexes is related to the difficulties encountered in the crystal growth of any crystal containing hexyl chains, which encouraged us to multiply the attempts on any sample available. In the present structure, like for **FFTRuCl$_2$NO**, a Ru^{II} is evidenced from the presence of one PF_6^- and one NO_2^-. The torsion angle between the mean planes of terpyridine and fluorene is equal to 31.16°, and 24.44° between the two fluorene units.

With the observation of *transoid* conformations between the fluorenes in **FFT** and **TFFT** and *cisoid* conformations in **FFTRuCl$_2$NO** and **FFC$_6$TRubpyNO$_2$**, the issue of conformation / property relationship in naturally addressed in these *bis*-fluorene based species. Although it is clear that packing effects may play the major role in the solid-state conformation, this issue will be reported in the next section.

2.4. Conformational aspects in bis-fluorene

The influence of the alkyl chains was investigated first. Replacing the CH_2 fragment of the fluorenes by alkyl chains of increasing lengths (increasing inductive effect) gradually enhances the overall donating capabilities of the whole fluorenyl substituent. Nevertheless, this effect is limited, and we have observed experimentally that replacing CH_2 by hexyl chains leads to a redshift of *ca.* 10 nm in **FC$_6$TRuClNO** [24]. For this reason, computations are usually performed on methylated fluorene, which accounts well

for the average donating effect along the series and maintain the duration of the computation under reasonable limits. Nevertheless, the influence of the chains on the *cisoid*/*transoid* conformation of *bis*-fluorene containing species deserves additional investigations due to possible interchains interactions. To clarify this issue, computations were performed on *bis*-fluorene molecules tetra-alkylated with alkyl chains C_i of various lengths, from i = 1 (Me) to i = 6 (He) within the framework of density functional theory (DFT). The comparison of the Gibbs free energy (G) is shown in Figure 5 as the difference $\Delta G = G_{transoid} - G_{cisoid}$. In any case, ΔG is positive, indicating the *cisoid* as the more stable conformation in solution. Interestingly, this trend is more pronounced as the length of the chain (*i*) becomes longer, which suggests that interchains interactions are a key parameter in the stabilization of the *cisoid* conformation. Nevertheless, and due to the modest energy difference (ΔG = 0.6 kcal/mol with tetra-hexylated species) the *cisoid*/*transoid* ratio is 73/27. Therefore, the presence of excited conformations cannot be avoided in solution. The rotation barrier calculated at the same DFT level is equal to 3.1 kcal.mol^{-1} for the *bis*-fluorene tetra-hexylated (i = 6), which is close to the 2.7 kcal.mol^{-1} computed for the biphenyl molecule as a reference. It indicates a nearly free rotation between the *cisoid*/*transoid* isomers (the scan of the energy profiles are presented in Supplementary Materials).

An additional comment arises, regarding the possibility of odd-even effect on ΔG and chain length, in Figure 6. Nevertheless, the examination of the DFT structures reveals that the C-H···H-C shortest distances between neighboring chains never implies CH located at the same position (*i*) along the chains. Therefore, great care should be taken to conclude on this point, which could deserve more investigation, implying the help of single-crystal structure investigations [33].

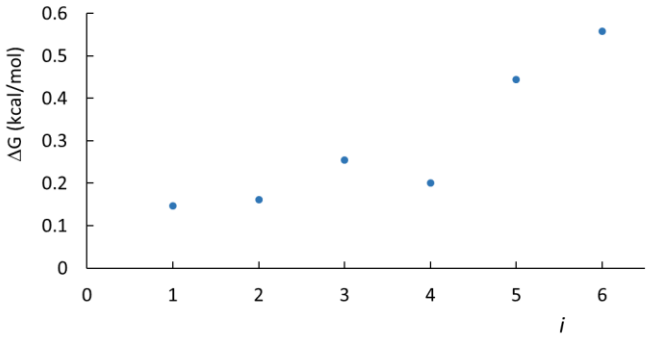

Fig. 6 Stabilization of the *cisoid* form ($\Delta G = G_{transoid} - G_{cisoid}$) in *bis*-fluorenes tetra substituted by alkyl chains of various lengths (*i*.= number of carbon atoms in the chains).

Once established that both conformations must be envisioned, their OPA and furthermore TPA spectra should be investigated as well, due to the final application of these RuNO complexes for light induced NO$^{\bullet}$ delivery. The computed ***bis*-(FC$_6$TRubpyNO)** OPA spectra are shown in Figure 7 for both *cisoid* and *transoid* conformations. The spectrum of the monometallic **FC$_6$TRubpyNO** is provided as a reference. In both mono- and bi-metallic species, the spectra are dominated by two bands, with a clear redshift of about 1500 cm^{-1}, for the bimetallic compounds, which can readily be ascribed to extended conjugation all over the molecular structures. Indeed, the computed torsion angles between the two fluorenes is equal to 35.6° and 40.5° for ***bis*-(FC$_6$TRubpyNO)** in *cisoid* and *transoid* conformations, respectively. It is known that the transfer integral between two π-subunits, and hence the overlap integral varies as the cosine of the torsion angle [34]. Therefore, values of 0.81 (cos 35.6°) and 0.76 (cos 40.5°) leads to a possibility of significant delocalization.

Data on the relevant transitions are summarized in Table 2. While the HOMO/LUMO frontier orbitals (167,168) pay the key role in **FC_6TRubpyNO**, it is interesting to observe that the relevant orbitals of the bimetallic species arise from combinations of those of the related monometallic fragments. This is further illustrated in Figure 7, where orbitals HOMO-1/HOMO 332-333 for the bimetallic ***bis*-(FC_6TRubpyNO)** are the odd and even combinations of 167 (monometallic), similarly LUMO/LUMO+1 (334-335 in the bimetallic) being related to 168 (monometallic), and finally LUMO+4/LUMO+5 (338-339) related to LUMO+2 (170) of the monometallic complex. The interaction between both monometallic subunits appears more pronounced in the *cisoid* form, leading to a slightly higher energy splitting (*e.g.* 332 *vs* 333). Nevertheless, this effect is very weak and one can assume that, to a large extent, the OPA properties of both *cisoid* and *transoid* isomers are the same.

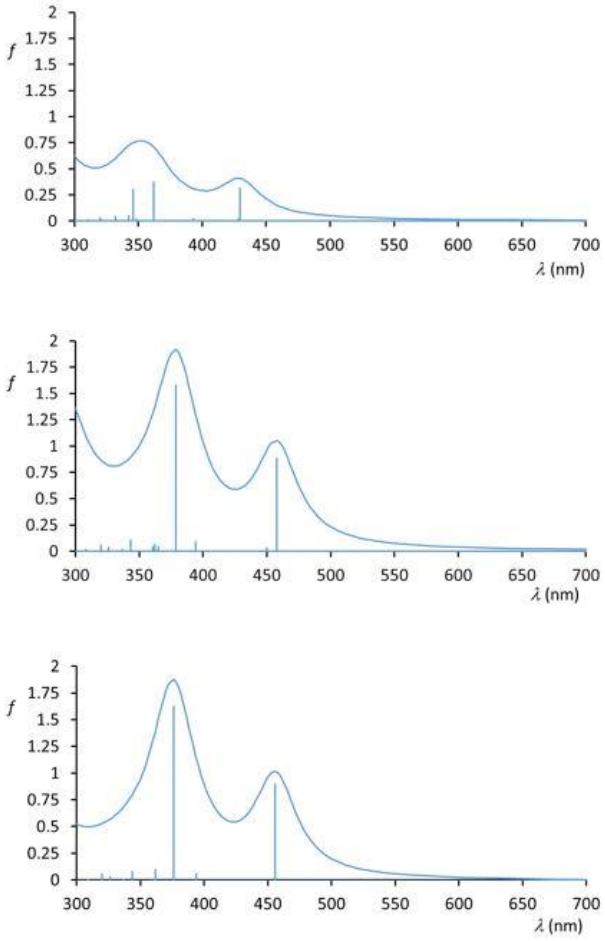

Fig. 7 TD-DFT computed spectra for **FC_6TRubpyNO** (top), ***bis*-(FC_6TRubpyNO)** in *cisoid* conformation (middle), and ***bis*-(FC_6TRubpyNO)** *transoid* conformation (bottom).

Table 2 Details of the relevant OPA transitions involved in **FC_6TRubpyNO**, and ***bis*-(**FC_6TRubpyNO)** in *cisoid* and *transoid* conformations, with absorption maxima (λ_{max} in nm), oscillator strengths (*f*), composition of the configuration expansion, and charge transfer character.

Compound	transition	λ_{max}	*f*	composition[1]	character
FC_6TRubpyNO	$1 \rightarrow 2$	430	0.314	78% $\chi_{167\rightarrow168}$	fluorene $\rightarrow$ RuNO
	$1 \rightarrow 7$	362	0.370	31% $\chi_{167\rightarrow170}$ + 19% $\chi_{164\rightarrow169}$	fluorene + ε terpy $\rightarrow$ RuNO + terpy
	$1 \rightarrow 9$	346	0.301	46% $\chi_{167\rightarrow170}$ + 21% $\chi_{164\rightarrow169}$	fluorene + ε terpy $\rightarrow$ RuNO + terpy
***bis*-(**FC_6TRubpyNO)**					
cisoid	$1 \rightarrow 2$	458	0.884	73% $\chi_{333\rightarrow334}$	fluorene $\rightarrow$ RuNO
	$1 \rightarrow 12$	379	1.578	53% $\chi_{333\rightarrow338}$ + 12% $\chi_{332\rightarrow339}$	fluorene $\rightarrow$ RuNO + terpy
transoid	$1 \rightarrow 2$	456	0.905	73% $\chi_{333\rightarrow334}$	fluorene $\rightarrow$ RuNO
	$1 \rightarrow 12$	376	1.623	52% $\chi_{333\rightarrow338}$ + 12% $\chi_{332\rightarrow339}$	fluorene $\rightarrow$ RuNO + terpy

[1] Orbital 167(168) is the HOMO(LUMO) in **FC_6TRubpyNO**, orbital 333(334) is the HOMO(LUMO) in ***bis*-(**FC_6TRubpyNO)**.

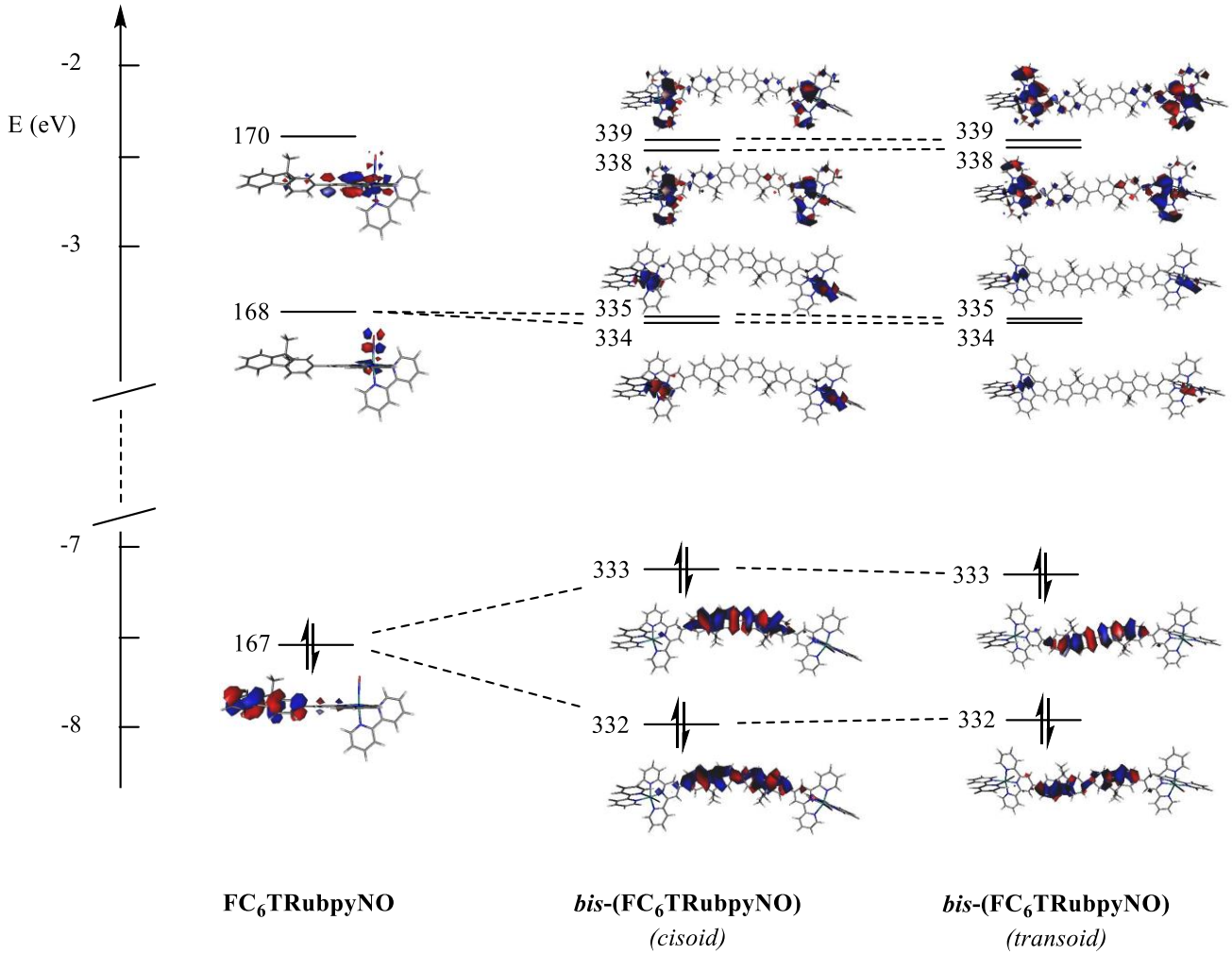

Fig. 7 Relevant orbitals in **FC_6TRubpyNO**, and ***bis*-(FC_6TRubpyNO)** (*cisoid* and *transoid* conformations). For the sake of simplification, hexyl chains are replaced by methyl chains.

Contrary to OPA spectra, the prediction of TPA spectra is a complicated task, which will not be described in the present contribution. Nevertheless, it may be recalled here that the molecular TPA response is quantified by the molecular cross-section (σ_{TPA}), which can be roughly regarded as the two-photon equivalent of the one-photon extinction coefficient (ε). Ultimately, σ_{TPA} is related to the second hyperpolarizability (γ), which can be evaluated within the framework of the perturbation theory, and expressed by an extensive sum-over-state expression [35], involving contribution of all $\langle m|\mu|n\rangle = \mu_{mn}$ OPA transitions between states *m* and *n*, through the following expression [25,27]:

$$\gamma_{ijkl} = \frac{1}{6\hbar^3} \times P(i,j,k,l) \times \left[\sum_{m\neq 0} \sum_{n\neq 0} \sum_{p\neq 0} \frac{\langle 0|\mu_i|m\rangle \langle m|\mu_j|n\rangle \langle n|\mu_k|p\rangle \langle p|\mu_l|0\rangle}{(\omega_{m0}-\omega-i\Gamma_{m0})(\omega_{n0}-2\omega-i\Gamma_{n0})(\omega_{p0}-\omega-i\Gamma_{p0})} - \sum_{m\neq 0} \sum_{n\neq 0} \frac{\langle 0|\mu_i|m\rangle \langle m|\mu_j|0\rangle \langle 0|\mu_k|n\rangle \langle n|\mu_l|0\rangle}{(\omega_{m0}-\omega-i\Gamma_{m0})(\omega_{n0}-\omega-i\Gamma_{n0})(\omega_{n0}+\omega-i\Gamma_{n0})} \right] \quad (1)$$

In this expression, *P* is a perturbation operator, *0*, *m*, *n*, *p* are the labels of the ground and excited states, *i*, *j*, *k*, *l* are molecular axes, $\hbar\omega_{m0}$ is the energy of state *m*, and Γ_{m0} is the band width of the $0 \rightarrow m$ transition. Clearly, Equation (1) encompasses the contribution of thousands of μ_{mn} terms and cannot be evaluated by a simple set of transitions. Nevertheless, all these terms are OPA transitions. Therefore, if two molecular entities exhibit strictly equivalent OPA spectra, their TPA spectra are necessarily the same. Applying this approach to the present case leads to the conclusion that, if the OPA spectra of ***bis*-(FC$_6$TRubpyNO)** in both *cisoid* and *transoid* forms are nearly the same, TPA spectra will be the same as well.

3 Conclusion

The synthesis of methylated (*bis*-fluorenyl)terpyridine and *bis*-(fluorenylterpyridine) ligands was achieved as an alternative to the previously reported hexylated ligands. This strategy allowed to easy achievement of crystal growth suitable for crystal structure determination. The structure examination indicates the possibility for both *cisoid* and *transoid* conformations for the *bis*-fluorene in the solid state. Quantum computations indicate that both conformations ca, be present in solution, however with a gradual stabilization of the *cisoid* forms when the length of the chains increases. The influence of the conformation is weak on the electronic transitions at both OPA and TPA levels.

4 Experimental

4.1. Starting materials and equipment

All starting materials were obtained from Alfa-Aesar and used without further purification. Analytical grade solvents were employed without any additional treatment. The starting dimethylated compound 9,9-dimethyl-7-bromofluorene-2-carbaldehyde (**1**) was obtained as described in the literature [30]. 9,9-dimethyl-2-bromofluorene (**5**) was purchased from Alfa-Aesar.

The sample of **FFC$_6$TRubpyNO$_2$** used for crystal growth experiments, which is an intermediate in the synthesis of **FFC$_6$TRubpyNO**, was obtained as previously reported [29]. Nuclear Magnetic Resonance (NMR) spectra were recorded at 298 K and 233 K on Bruker Avance III 300/400 spectrometers using

deuterated solvents. Chemical shifts for ^{1}H and ^{13}C NMR data are referenced relative to the residual nondeuterated solvent signal, fixed at δ = 7.26 ($CDCl_3$), δ = 5.32 (CD_2Cl_2) ppm for ^{1}H-NMR and d = 77.00 ($CDCl_3$), δ = 53.84 (CD_2Cl_2) ppm for ^{13}C-NMR. Coupling constants (J values) are reported in Hertz. High-Resolution Mass Spectrometry (HRMS) data were acquired using an Xevo G2 Q TOF (Waters) UPLC spectrometer. In the HRMS data, "M" denotes the molecular ion for organic molecules and neutral complexes, or the cation for ionic coordination compounds. The NMR spectra of the ligands and intermediates are provided in Supplementary Materials (10 spectra).

4.2. Synthesis

(E)-3-(9,9-methyl-7-bromo-fluoren-2-yl)-1-(pyridin-2-yl)prop-2-en-1-one. (2)

To a round-bottom flask containing 9,9-dimethyl-7-bromofluorene-2-carbaldehyde (1) (3.0010 g, 10.0 mmol), 2-acetylpyridine (2.93 mL, 6.1 mmol), ethanol (60 mL), and THF (2.0 mL), aqueous NaOH (10 mL, 0.1 M) was slowly added under magnetic stirring. The mixture was stirred at room temperature for 7 hours. Following this, the resulting yellow solid was collected, washed with water, and subjected to recrystallization from ethanol. This process yielded 2.6700 g (6.6 mmol, 66.2%) of compound (2) as a yellow solid. **^{1}H-NMR.** (300 MHz, $CDCl_3$) δ 8.78 (ddd, J = 4.7, 1.8, 0.9 Hz, 1H), 8.33 (d, J = 16.0 Hz, 1H), 8.25 – 8.19 (m, 1H), 8.03 (d, J = 15.9 Hz, 1H), 7.90 (td, J = 7.7, 1.7 Hz, 1H), 7.80 (t, J = 1.4 Hz, 1H), 7.71 (t, J = 1.2 Hz, 2H), 7.62 – 7.57 (m, 2H), 7.55 – 7.50 (m, 1H), 7.48 (dd, J = 8.0, 1.9 Hz, 1H), 1.53 (s, 6H). **^{13}C-NMR** (100 MHz, $CDCl_3$) δ 189.34, 156.35, 154.37, 153.85, 148.84, 145.16, 140.87, 137.38, 137.09, 134.64, 130.37, 129.12, 126.90, 126.31, 123.01, 122.58, 122.01, 121.87, 120.44, 120.14, 47.17, 26.95. **HRMS** (ESI-TOF^{+}) m/z anal. calcd. For $C_{23}H_{18}BrNO$ $[M+H]^{+}$: 404.0644. Found: 404.0642. Error: 0.5 ppm.

4'-(9,9-dimethyl-7-bromo-fluoren-2-yl)-2,2':6',2''-terpyridine. (3).

In a round-bottom flask, 1-[2-oxo-2-(2-pyridyl)ethyl]pyridinium iodide (2.0350 g, 6.2 mmol), compound **2** (2.5000 g, 6.2 mmol), and NH_4OAc (4.7750 g, 62.0 mmol) were combined with ethanol (50 mL) and THF (25 mL). The mixture was refluxed for 24 hours. Following this, the resulting green solid was collected, washed with water, and subjected to purification by column chromatography on silica gel using pentane/ethyl acetate (9:1) as the eluent. This purification process yielded 1.7000 g (3.3790 mmol, 54.5%) of compound **3** as a crystalline yellow solid. **^{1}H-NMR.** (300 MHz, $CDCl_3$) δ 8.81 – 8.75 (m, 4H), 8.70 (dt, J = 8.0, 1.0 Hz, 2H), 7.97 – 7.87 (m, 4H), 7.82 (dd, J = 7.9, 0.7 Hz, 1H), 7.68 – 7.58 (m, 2H), 7.50 (dd, J = 8.1, 1.9 Hz, 1H), 7.42 – 7.36 (m, 2H), 1.58 (s, 6H). **^{13}C-NMR** (100 MHz, $CDCl_3$) δ 156.35, 155.91, 155.11, 153.32, 150.74, 149.11, 141.54, 139.97, 138.06, 136.94, 134.01, 128.84, 126.62, 123.84, 121.58, 121.48, 120.91, 119.69, 118.96, 83.81, 47.18, 27.14, 25.03, 24.93. **HRMS** (ESI-TOF^{+}) m/z anal. calcd. For $C_{30}H_{22}BrN_3$ $[M+H]^{+}$: 504.1075. Found: 504.1080. Error: 0.5 ppm.

4'-(9,9-dimethyl-7-(4,4,5,5-tetramethyl-1,3,2-dioxaborolan-2-yl)-fluoren-2-yl)-2,2':6',2''-terpyridine. **(4)**.

In a 5 mL Schlenk flask, compound **3** (2.2052 g, 4.4 mmol), bis(pinacolato)diboron (2.0501 g, 8.1 mmol), potassium acetate (2.3710 g, 24.1 mmol), and DMSO (40 mL) were combined. The resulting mixture was made heterogeneous by sparging with argon for 15 minutes. Subsequently, $Pd(dppf)Cl_2$·DCM (0.3001 g, 0.37 mmol) was added. The reaction mixture was heated at 110°C for 24 hours, then cooled to room temperature. After filtration, the mixture was extracted with chloroform, washed with brine, and dried using anhydrous Na_2SO_4. The solvent was removed under reduced

pressure, and column chromatography on silica gel using pentane/ethyl acetate (7:3) as the eluent was performed. This purification process yielded 1.5 g (2.7 mmol, 61.8%) of compound **4** as a yellow powder. **^{1}H-NMR.** (300 MHz, Chloroform-d (300 MHz, CDCl3) δ 8.79 (s, 2H), 8.77 – 8.74 (m, 2H), 8.69 (dt, J = 7.9, 1.2 Hz, 2H), 7.96 – 7.95 (m, 1H), 7.93 – 7.84 (m, 6H), 7.79 (dd, J = 7.6, 0.8 Hz, 1H), 7.37 (ddd, J = 7.5, 4.8, 1.3 Hz, 2H), 1.60 (s, 6H), 1.39 (s, 12H). **^{13}C-NMR**. (100 MHz, $CDCl_3$) δ 156.35, 155.91, 155.11, 153.32, 150.74, 149.11, 141.54, 139.97, 138.06, 136.94, 134.01, 128.84, 126.62, 123.84, 121.58, 121.48, 120.91, 119.69, 118.96, 83.81, 47.18, 27.14, 25.03, 24.93. **HRMS** (ESI-TOF^{+}) m/z anal. calcd. For $C_{36}H_{34}BN_3O_2$ $[M+H]^{+}$: 552.2844. Found: 552.27. Error: -0.6 ppm.

TFFT

To a Schlenk flask were added **4** (1.0024 g, 1.8 mmol), **3** (0.9200 g, 1.81 mmol), K_2CO_3 (0.08202 g, 5.97 mmol), tetra-n-butyl ammonium bromide (0.2470 g, 0.077 mmol), and $Pd(dppf)_2Cl_2$ (0.6270 g, 0.767 mmol). After purging the system with argon, a 10/1/0.5 toluene/ethano/DCM mixture (20 mL) was added, followed by magnetic stirring at reflux temperature for 24 hours. The product was chilled to room temperature, filtered and purified by column chromatography using silica gel and dichloromethane/ethyl acetate (8/2) as eluent to yield 0.3803 g (0.45 mmol, 24.8 %) of **Ligand TFFT** as a red solid. **^{1}H-NMR.** (300 MHz, CD_2Cl_2) δ 8.85 (s, 4H), 8.77 – 8.72 (m, 6H), 8.71 (t, J = 1.1 Hz, 2H), 8.03 (t, J = 1.2 Hz, 2H), 7.95 (d, J = 1.2 Hz, 4H), 7.94 – 7.88 (m, 6H), 7.83 (d, J = 1.1 Hz, 2H), 7.75 (dd, J = 7.9, 1.7 Hz, 2H), 7.40 (ddd, J = 7.5, 4.8, 1.2 Hz, 4H), 1.69 (s, 12H). **^{13}C-NMR.** (100 MHz, CD_2Cl_2) δ 156.71, 156.42, 155.60, 151.22, 149.44, 141.74, 140.71, 138.31, 138.02, 137.77, 126.95, 126.92, 124.72, 122.36, 122.05, 122.00, 121.25, 121.19, 119.25, 47.77, 27.40. **HRMS** (ESI-TOF^{+}) m/z anal. calcd. For $C_{80}H_{85}N_6$ $[M+H]^{+}$: 1129.6836. Found: 1129.6846. Error: 0.9 ppm.

FFT

Prepared as described above for **Ligand TFFT** from **(5)**. Yield: 45 % (Pale yellow solid). **^{1}H-NMR.** (400 MHz, $CDCl_3$) δ 8.81 (s, 2H), 8.77 (dd, *J* = 4.8, 0.9 Hz, 2H), 8.71 (dt, *J* = 8.0, 1.2 Hz, 2H), 7.99 (d, *J* = 1.8 Hz, 2H), 7.95 – 7.87 (m, 1H), 7.87 – 7.81 (m, 4H), 7.78 (dd, *J* = 7.4, 1.4 Hz, 2H), 7.73 (dd, *J* = 7.9, 1.7 Hz, 1H), 7.68 (td, *J* = 7.9, 1.7 Hz, 2H), 7.48 (dd, *J* = 7.2, 1.5 Hz, 1H), 7.42 – 7.33 (m, 4H), 1.67 (s, 6H), 1.58 (s, 6H). **^{13}C-NMR.** (100 MHz, CDCl3) δ 156.56, 156.10, 155.03, 154.86, 154.47, 154.07, 150.93, 149.30, 141.44, 140.89, 140.07, 139.03, 138.63, 137.89, 137.70, 137.07, 127.41, 127.19, 126.88, 126.62, 126.48, 123.99, 122.78, 121.69, 121.65, 121.62, 121.60, 120.81, 120.65, 120.46, 120.23, 119.06, 47.45, 47.15, 27.49, 27.43. **HRMS** (ESI-TOF^{+}) m/z anal. calcd. For $C_{45}H_{35}N_3$ $[M+H]^{+}$: 618.2836 Found: 618.2830. Error: -0.15 ppm.

FFTRuCl$_2$NO

A mixture of **FFT** (0.408 mg, 0,66 mmol), $RuCl_3 \cdot xH_2O$ (0.263mg, 0.66 mmol) and ethanol (50 mL) was stirred under reflux for 3 hours, which was subsequently filtered under vacuum, washed with ethanol and a small amount of diethyl ether. The final [Ru^{III}(**FFT**)(Cl_3)] solid was obtained as a black powder with a yield of 95%.

[Ru^{III}(**FFT**)(Cl_3)] (165 mg, 0.2 mmol) was dissolved in dimethylformamide (15 mL) and heated to 80 °C. Gaseous nitric oxide, generated by dropwise addition of diluted HNO_3 onto copper, was bubbled through the solution under argon atmosphere for 3 hours. The reaction mixture was then allowed to cool down to room temperature, leading to the formation of a precipitate corresponding to the *trans* isomer. It was isolated through vacuum filtration and obtained as an orange solid (93 mg, 54.4 % yield). The remaining filtrate was evaporated under vacuum and the *cis*/*trans* resulting mixture was separated by HPLC using an apolar X Bridge C18 column as

the stationary phase. The mobile phase was a mixture of acetonitrile with 1% trifluoroacetic acid (TFA) and water with 1% TFA. The yield after separation was 3% for *cis*(Cl,Cl)-[Ru^{II}(**FFT**)(Cl_2)(NO)](Cl) and 49% for *trans*(Cl,Cl)-[Ru^{II}(**FFT**)(Cl_2)(NO)](Cl). The Cl^- counter ions were then replaced by PF_6^- through metathesis reaction. The complex was solubilized in a minimum of DMF (0.16 mmol in 10 mL DMF) and a large excess of NH_4PF_6 (350 mg in 30 mL of water) was added. The resulting precipitate was filtered under vacuum and rinsed with water, ethanol and ether.

cis(Cl,Cl)-[Ru^{II}(**FFT**)(Cl_2)(NO)]PF_6. **^{1}H-NMR**. (300 MHz, CD_3CN, 298 K): δ (ppm) 9,24 (2H, dd, J= 5,4 Hz, 1,3 Hz), 8,95 (2H, s), 8,84 (2H, d, J= 7,9 Hz), 8,55 (2H, td, J= 8,0 Hz, 1,5 Hz), 8,35 (1H, s), 8,20-8,16 (2H, m), 8,08-7,77 (9H, m), 7,61-7,57 (1H, m), 7,44-7,39 (2H, m), 1,75 (6H, s), 1,60 (6H, s). **HRMS** (ESI-TOF^+) m/z anal. calcd. For $C_{45}H_{35}Cl_2N_4ORu$ $[M]^+$: 819.1231 Found: 819.1243. Error: 1.5 ppm.). **IR(ATR)**: νNO=1897 cm^{-1}.

trans(Cl,Cl)-[Ru^{II}(**FFT**)(Cl_2)(NO)]PF_6. **^{1}H-NMR**. (300 MHz, CD_3CN, 298 K): δ (ppm) 8,87 (2H, s), 8,81 (4H, m), 8,46 (2H, td, J= 7,9 Hz, 1,4 Hz), 8,33 (1H, s), 8,16 (2H, s), 8,08-7,77 (8H, m), 7,61-7,57 (2H, m), 7,43-7,39 (2H, m), 1,73 (6H, s), 1,59 (6H, s). **^{13}C-NMR** (100 MHz, CD_3CN) δ 157.63, 156.63, 156.56, 156.19, 155.65, 155.14, 155.10, 154.08, 143.95, 143.50, 143.06, 141.09, 139.66, 139.54, 137.79, 134.59, 131.04, 128.96, 128.62, 128.23, 127.63, 127.30, 124.05, 123.79, 123.58, 122.69, 122.66, 122.58, 122.31, 121.55, 121.24, 48.42, 47.88, 27.35, 27.21. **HRMS** (ESI-TOF^+) m/z anal. calcd. For $C_{45}H_{35}Cl_2N_4ORu$ $[M]^+$: 819.1231 Found: 819.1223. Error: -1.0 ppm. **IR(ATR)**: νNO=1904 cm^{-1}.

4. 3. X-Ray Diffraction Studies

Single crystals suitable for X-ray crystal structure investigations were grown by slow diffusion of diethylether in concentrated solution of ligands in CH_2Cl_2 or ruthenium complexes in acetonitrile.

Data were collected on a Bruker Kappa Apex II diffractometer equipped with a 30 W air-cooled microfocus source using MoKα radiation (λ = 0.71073 Å) for **FFT**, **FFTRuCl$_2$NO**, and **FFC$_6$TRubpyNO$_2$**, and on an Oxford Diffraction GEMINI diffractometer using CuKα radiation (λ = 1.54184 Å) for **TFFT**. Cooling devices were used to collect the data at low temperature between 100(2) and 193(2) K. Phi and Omega scans were performed for data collection, an empirical absorption correction was applied and the structures were solved by intrinsic phasing method (ShelXT) [36]. All non-hydrogen atoms were refined anisotropically by means of least-squares procedures on F^2 with ShelXL [37]. All the hydrogen atoms were refined isotropically at calculated positions using a riding model with their isotropic displacement parameters constrained to be equal to 1.5 times the equivalent isotropic displacement parameters of their pivot atoms for terminal sp3 carbon and 1.2 times for all other carbon atoms. For **TFFT**, the SQUEEZE [38] function of PLATON was used to remove the electron density contribution of the highly disordered solvent molecules. And for **FFC$_6$TRubpyNO$_2$**, the crystal structure with only NO_2 coordinated to the Ru atom was not fully acceptable. Anisotropic displacements parameters and the residual electron density suggested a disorder between the NO_2 group and a Cl atom in a ratio 84:16 after refinement. For this structure, the highest peak in the final difference map is only 0.61 e/A^3 at 1.06 Å from the F2 atom of the PF_6^- counter-anion. All the residual density is close to the PF_6^- or the molecule, so no solvent model could be found.

X-Ray data (atomic coordinated, bond lengths and angles) are provided in Supplementary Materials. The four crystal structures (CIF format) were deposited with the Cambridge Crystallographic Data

Center, with the following numbers: CCDC 2283492 (**FFT**), 2283493 (**TFFT**), 2283494 (**FFTRuCl$_2$NO**),and 2283495 (**FFC$_6$TRubpyNO$_2$**).

4.4. Computational methods

The molecular geometries of the six *bis*-fluorene tetrasubstituted by (C_i) alkyl chains of various lengths (i = 1 to 6) were fully optimized using the Gaussian-09 program package [39] within the framework of the DFT at the B3PW91/6-31G* level. The B3PW91/6-31G* method was selected for consistency with our previous investigation devoted to chromophores containing fluorene units [24,29,32,40], and because it was reported to outperform other hybrid functionals (*e.g.* B3LYP) or pure functionals (*e.g.* PW91) for RuNO complexes [41]. Solvent effects were included by using the polarizable continuum model (PCM) implemented in Gaussian09 for acetonitrile (ε = 35.688). Vibrational analysis was performed at the same level to verify that the stationary points correspond to minima on the potential energy surfaces. For each molecule, *cisoid* and *transoid* conformations were envisioned. The relative stability of both conformations was determined by comparison of their Gibbs free energies. The TD-DFT computations of the UV-vis spectra were carried out on the optimized geometries at the CAM-B3LYP/6-31G* level, for consistency with our previous investigations [24,29,32,39,42], and because it is well designed for providing a good agreement with experimental data in the case of electronic systems with long-range charge transfers capabilities [43]. This long-range corrected hybrid functional is also reported as being particularly well suited for studying molecules with very delocalized excited states [44]. Similarly, **FC$_6$TRubpyNO** and ***bis*-(FC$_6$TRubpyNO)** (*cisoid* and *transoid* isomers) were optimized at the B3PW91/6-31G* level and there spectra computed at the CAM-B3LYP/6-31G* level, using acetonitrile as the solvent. The coordinates of the 15 molecular structures are provided in Supplementary Materials.

Acknowledgements.

P. L.-V. acknowledges support from the French National Research Agency under program ANR-18-CE29-0012. MB thanks the University Paul Sabatier (COMUE) and the Région Midi-Pyrénées for the RuNOthérapie grant.

Appendix A. Supplementary data

NMR spectra, DFT geometries, scan energy profiles.

CCDC contains the supplementary crystallographic data for FFT (2283492), TFFT (2283493), FFTRuCl$_2$NO (2283494) and FFC$_6$TRubpyNO$_2$ (2283495). These data can be obtained free of charge via http://www.ccdc.cam.ac.uk/conts/retrieving.html, or from the Cambridge Crystallographic Data Centre, 12 Union Road, Cambridge CB2 1EZ, UK; fax: (+44) 1223-336-033; or e-mail: deposit@ccdc.cam.ac.uk.

References

[1] J. O. Lundberg, E. Weitzberg, *Cell* **2022**, *185*, 2853-2878.
[2] H. Alimoradi, K. Greish, A. B. Gamble, G. I. Giles, *Pharm. Nanotechnol.* **2019**, *7*, 279-303
[3] S. Hossain, L. M. Nisbett, E. M. Boon, *Acc. Chem. Res.* **2017**, *50*, 1633– 163

[4] P. C. Ford, *Nitric Oxide*, **2013**, *34*, 56-64.
[5] L. J. Ignarro, *Nitric Oxide Biology and Pathobiology*, Academic Press, San Diego, **2000**.
[6] W.H. Poh, S.A. Rice, *Molecules* **2022**, *27*, 674-712.
[7] S. Paul, S. Pan, A. Mukherjee, P. De, *Mol. Pharma.* 2021, 18, 3181-3202.
[8] M. Wu, Z. Lu, K. Wu, C. Nam, L. Zhang, J. Guo, *J. Mater. Chem. B* **2021**, *9*, 7063-7975.
[9] E. Zoupa, N. Pitsikas, *Molecules* **2021**, *26*, 3196.
[10] Y. Yang, Z. Huang, L.L. Li, *Nanoscale* **2021**, *13*, 444-459.
[11] M. Paulo, D. E. F. R. Costa, D. Bonaventura, C. N. Lunardi, L. M. Bendhack, *Current Pharma. Design* **2020**, *26*, 3748-3759.
[12] C. Porrini, N. Ramarao, S. Tran., *Bio. Chem.* **2020**, *401*, 547-572
[13] M. D. Brown, M. H. Schoenfisch, *Chem. Rev.* **2019**, *119*, 11551-11575.
[14] D. D. Thomas, L. A. Ridnour, J. S. Isenberg, W. Flores-Santana, Ch. H. Switzer, S Donzellie, P. Hussain, C. Vecoli, N. Paolocci, S. Ambs, C. Colton, C. Harris, D. D. Roberts, D. A. Wink, *Free Radic. Biol. Med.* **2008**, *45*, 18-31.
[15] S. Mocellin, V. Bronte, D. Nitti, *Med. Res. Rev.* **2007**, *27*, 317-352.
[16] I. Stepanenko, M. Zalibera, D. Schaniel, J. Telser, V. B. Arion, *Dalton Trans.* **2022**, *51*, 5367-5393.
[17] (a) N. L. Fry, P. K. Mascharak, *Acc. Chem. Res.* **2011**, *44*, 289-298.
(b) M. J. Rose, P. K. Mascharak, *Coord. Chem. Rev.* **2008**, *252*, 2093-2114.
[18] R. Santana da Silva, R. Galvao de Lima, S. P. Machado, *Adv. Inorg. Chem.* **2015**, *67*, 265-294.
[19] P. C. Ford, *Acc. Chem. Res.*, **2008**, *41*, 190–200
[20] for recent reports on ruthenium nitrosyl complexes with NO˙ releasing capabilities, see:
(a) N. Sharma, V. Kumar, D. Amilan Jose, *Dalton Trans.* **2023**, *52*, 675-682.
(b) L.B. Dela Rosa, J.H. Jorolan, *Asian J. Chem.* **2023**, *35* 52-56.
(c) A. Ferrarini, R. N. Soek, R. Rebecchi Rios, F. S. Santana, R. B. Campos, R. S. da Silva, F. S. Nunes, *Inorg. Chim. Acta* **2022**, *533*, 120771.
F. Ma, T.T. Zhang, Z.H. Zhang, H.X. Tong, X.Y. Yi, *Inorg. Chim. Acta* (2022), 534, 120826
(d) J.-H. Cho, M. Kim, Y. You, H.-I. Lee, *Chem. Asian J.* **2022**, *17*, e202101244.
(e) I. Stepanenko, P. Mizetskyi, E. Orlowska, L. Bucinsky, M. Zalibera, B. Venosova, M. Clemancey, G. Blondin, P. Rapta, G. Novitchi, W. Schrader, D. Schaniel, Y.-S. Chen, M. Lutz, J. Telser, V. B. Arion, *Inorg. Chem.* **2022**, *61*, 950-967.
(f) N. Sharma, P. Arjunan, S. Marepally, N. Jain, A. R. Naziruddin, A. Ghosh, C. R. Mariappan, J. D. Amilan, *J. Photochem. Photobiol. A* **2022**, *425*, 113703.
(g) A.A. Mikhailov, G.A. Kostin, D. Schaniel, Dominik, *New J. Chem.* **2022**, *46*, 12641-12650.
(h) Y. Wu, Y. Wang, Y. Sun, Z. Li, X. Li, Z. Zhou, D. Tang, *Inorg. Chem.* **2022**, *61*, 8997-9011.
(i) S. Singh, G.R. Navale, M. Mahale, V. K. Chaudhary, K. Kodam, K. Ghosh, *Nitric Oxide* **2022**, *129*, 30-40.
[21] M. R. Hamblin, T. N. Demidova, *Proc. SPIE, Mechanism for Low-Light Therapy* **2006**, 6140, 614001–614012.
[22] B. Strehmel, V. Strehmel, *Adv. Photochem.*, **2007**, *29*, 111-341.
[23] M. Pawlicki, H. A. Collins, R. G. Denning, H. L. Anderson, *Angew. Chem. Int. Ed.*, **2009**, *48*, 3244-3266.
[24] A. Enriquez-Cabrera, I. Sasaki, V. Bukhanko, M. Tassé, S. Mallet-Ladeira, P. G. Lacroix, R. M. Barba-Barba, G. Ramos-Ortiz, N. Farfán, Z. Voitenko, I. Malfant, *Eur. J. Inorg. Chem.* **2017**, *2017*, 1446-1456.
[25] F. Terenziani, C. Katan, E. Badaeva, S. Tretiak, M. Blanchard-Desce, *Adv. Mater.*, **2008**, *20*, 4641-4678.
[26] G. S. He, L.-S. Tan, Q. Zheng, P. N. Prasad, *Chem. Rev.*, **2008**, *108*, 1245-1330.

[27] Ch. Andraud, R. Fortrie, C. Barsu, O. Stéphan, H. Chermette, P. L. Baldeck, *Adv. Polym. Sci.*, **2008**, *214*, 149-203.

[28] M. Albota, D. Beljonne, J. L. Bredas, J. E. Ehrlich, J. Y. Fu, A. A. Heikal, S. E. Hess, T. Kogej, M. D. Levin, S. R. Marder, D. McCord-Maughon, J. W. Perry, H. Rockel, M. Rumi, G. Subramaniam, W. W. Webb, X. L. Wu, C. Xu, *Science* **1998**, *281*, 1653-1656.

[29] Y. Juarez-Martinez, P. Labra-Vázquez, A. Enríquez-Cabrera, A.F. Leon-Rojas, D. Martínez-Bourget, P.G. Lacroix, M. Tassé, S. Mallet-Ladeira, N. Farfán, R. Santillan, G. Ramos-Ortiz, J.-P. Malval, I. Malfant, *Chem. Eur. J.*, **2022**, e202201692 (1-14).

[30] D. Göbel, M. Friedrich, E. Lork, B. J. Nachtsheim, *Beilstein J. Org. Chem.* **2020**, *16*, 1683-1692.

[31] F. Kröhnke, W. Zecher, J. Curtze, D. Drechsler, K. Pfleghar, K. E. Schnalke, W. Weis, *Angew. Chem.Int. Ed. Engl.* **1962**, *1*, 626–632.

[32] (a) J. Akl, I Sasaki, P.G. Lacroix, I. Malfant, S. Mallet-Ladeira, P. Vicendo, N. Farfán, R. Santillan, *Dalton Trans.* **2014**, *45*, 12721-12733. (b) J. Akl, I. Sasaki, P.G. Lacroix, V. Hugues, P. Vivendo, M. Bocé, S. Mallet-Ladeira, M. Blanchard-Desce, I. Malfant, *Photochem. Photobio. Sci.* **2016**, *15*, 1484-1491.

[33] N. Suzuki, T. Matsuda, T. Nagai, K. Yamazaki, M. Fujiki, Cryst. Growth Des. 2016, 16, 6593-6599.

[34] R. Chauvin, Ch. Lepetit, *Phys. Chem. Chem. Phys.* **2013**, *15*, 3855-3830, and references herein.

[35] B. J. Orr, J. F. Ward, *Mol. Phys.*, **1971**, *20*, 513-526.

[36] SHELXT: G. M. Sheldrick, University of Göttingen, *Acta Crystallogr. Sect. A*, **2015**, *71*, 3-8.

[37] SHELXL, G. M. Sheldrick, University of Göttingen, *Acta Crystallogr. Sect. C*, **2015**, *71*, 3-8.

[38] A. L. Spek, *Acta Crystallogr. Sect. C*, **2015**, 71, 9-18.

[39] Gaussian 09, Revision E.01, M. J. Frisch, G. W. Trucks, H. B. Schlegel, G. E. Scuseria, M. A. Robb, J. R. Cheeseman, G. Scalmani, V. Barone, B. Mennucci, G. A. Petersson, H. Nakatsuji, M. Caricato, X. Li, H. P. Hratchian, A. F. Izmaylov, J. Bloino, G. Zheng, J. L. Sonnenberg, M. Hada, M. Ehara, K. Toyota, R. Fukuda, J. Hasegawa, M. Ishida, T. Nakajima, Y. Honda, O. Kitao, H. Nakai, T. Vreven, J. A. Montgomery, Jr., J. E. Peralta, F. Ogliaro, M. Bearpark, J. J. Heyd, E. Brothers, K. N. Kudin, V. N. Staroverov, R. Kobayashi, J. Normand, K. Raghavachari, A. Rendell, J. C. Burant, S. S. Iyengar, J. Tomasi, M. Cossi, N. Rega, J. M. Millam, M. Klene, J. E. Knox, J. B. Cross, V. Bakken, C. Adamo, J. Jaramillo, R. Gomperts, R. E. Stratmann, O. Yazyev, A. J. Austin, R. Cammi, C. Pomelli, J. W. Ochterski, R. L. Martin, K. Morokuma, V. G. Zakrzewski, G. A. Voth, P. Salvador, J. J. Dannenberg, S. Dapprich, A. D. Daniels, Ö. Farkas, J. B. Foresman, J. V. Ortiz, J. Cioslowski, and D. J. Fox, Gaussian, Inc., Wallingford CT, **2009**.

[40] (c) M. Roose, I. Sasaki, V. Bukhanko, S. Mallet-Ladeira, R.M. Barba-Barba, G. Ramos-Ortiz, A. Enriquez-Cabrera, N. Farfán, P.G. Lacroix, I. Malfant, *Polyhedron* **2018**, 151, 100-111.

[41] M.J. Rose, P.K. Mascharak, *Inorg. Chem.* **2009**, *48*, 6904-6917.

[42] (a) V. Bukhanko, P. G. Lacroix, I. Sasaki, M. Tassé, S. Mallet-Ladeira, Z. Voitenko, I. Malfant, *Inorg. Chim. Acta* **2018**, *482*, 195-205. (b) M. Roose, M. Tassé, P. G. Lacroix, I. Malfant, *New J. Chem.* **2019**, *43*, 755-767. (c) V. Bukhanko, A. F. León-Rojas, P. G. Lacroix, M. Tassé, G. Ramos-Ortiz, R. M. Barba-Barba, N. Farfán, R. Santillan, I. Malfant, *Eur. J. Inorg. Chem.* **2021**, 1670-1684.

[43] T. Yanai, D. Tew, and N. Handy, *Chem. Phys. Lett.*, **2004**, *393*, 51-57.

[44] D. Jacquemin, E. A. Perpète, G. E. Scuseria, I. Ciofini, C. Adamo, *J. Chem. Theory Comput.* **2008**, *4*, 123-135